Available online at www.sciencedirect.com
SCIENCE DIRECT
ELSEVIER
Palaeogeography, Palaeoclimatology, Palaeoecology 234 (2006) 201–222
PALAEO
www.elsevier.com/locate/palaeo

Environmental changes at the eastern Namib Desert margin before and after the Last Glacial Maximum: New evidence from fluvial deposits in the upper Hoanib River catchment, northwestern Namibia

Bernhard Eitel [a,*], Annette Kadereit [b], Wolf-Dieter Blümel [c], Klaus Hüser [d], Johanna Lomax [e], Alexandra Hilgers [e]

[a] *Department of Geography, University of Heidelberg, INF 348, D-69120 Heidelberg, Germany*
[b] *Forschungsstelle Archäometrie der Heidelberger Akademie der Wissenschaften am Max-Planck-Institut für Kernphysik, Saupfercheckweg 1, D-69117 Heidelberg, Germany*
[c] *Geographical Institute, University of Stuttgart, Azenbergstr. 12, D-70174 Stuttgart, Germany*
[d] *Department of Geosciences, Universität Bayreuth, Universitätsstr. 30, D-95447 Bayreuth, Germany*
[e] *Geographical Institute, University of Cologne, Albertus-Magnus-Platz , D-50923 Köln, Germany*

Received 20 December 2004; received in revised form 3 October 2005; accepted 13 October 2005

Abstract

In the upper Hoanib River catchment area, northwestern Namibia, fine-grained silty deposits are widespread. Accumulated as river-end deposits they form excellent geomorphological archives of a highly sensitive desert-margin area. Different sedimentary complexes are separated sedimentologically and by luminescence dating. The deposits give evidence of climate oscillations at the eastern margin of the Namib Desert during the past 50,000 years.

In northwestern Namibia, the dry conditions of the desert-margin area with less than 200–300 mm mean annual precipitation prevailed at ~60–40 ka and at ~34–24 ka when sediment complex-I accumulated. During the Last Glacial Maximum (LGM), fluvial activity and sedimentation were most likely interrupted due to arid conditions. Between ~12 ka and the Mid-Holocene higher rainfall and runoff led to the aggradation of sediment complex-II. The climate was more humid than before the LGM, but drier than at present. After ~3 ka runoff increased and the Hoanib River re-eroded the older deposits forming deep channels. A prominent, more sandy and gravely 4 m-terrace in the upper and middle course of the Hoanib River dates to the Little Ice Age (LIA). It is likely that this terrace is genetically linked with the Amspoort Silt formation in the Lower Hoanib valley.

Keywords: Namibia; Namib Desert; Hoanib River; Dryland geomorphology; OSL-dating; Quaternary

1. Introduction

Northwestern Namibia is characterized by a prominent hygric gradient of ~20 mm mean annual precipitation per 10 km which decreases from the semi-arid highlands west of the Etosha Basin (>250 mm mean annual rainfall) to the hyperarid northern Namib Desert extending at the Atlantic coast. The aridity is caused by a quasi-stationary high-pressure cell over the southern Atlantic Ocean and the offshore upwelling Benguela circulation. Stable atmospheric layering results from dynamic inversion due to subsiding air, which is reinforced by cool sea surface temperatures, usually be-

* Corresponding author. Tel.: +49 6221 54 4543.
E-mail address: bernhard.eitel@urz.uni-heidelberg.de (B. Eitel).

0031-0182/$ - see front matter © 2005 Elsevier B.V. All rights reserved.
doi:10.1016/j.palaeo.2005.10.015

tween 11 and 17 °C (Van der Merve, 1983). Thus, both the marine and the atmospheric system restrict convection and prevent the formation of high clouds.

The transition zone between the savanna, that receives monsoonal summer rain, and the coastal desert reacts sensitively to changing rainfall quantities and intensities. Therefore, the northern Namib Desert margin is one of the geomorphologically most responsive regions on Earth. Sensitive areas like this are known to record and store detailed proxies of rapid environmental changes within the sediments and soils. This is the reason why an increasing number of palaeoenvironmental studies has been taken up in northwestern Namibia over the past decade (see compilation in Eitel et al., 2002). During the same time optical dating of sediments has made rapid progress (e.g. Grün and Wintle, 2003). In arid regions limited availability of organic matter implies difficulties in the application of radiocarbon dating and luminescence dating often proves to be an indispensable chronometric technique to arid palaeoenvironmental reconstruction from sedimentary archives.

In northwestern Namibia the desert margin is geomorphologically marked by the Great Escarpment. This separates the highland plains (~1200 m a.s.l.) to the east from the mountainous region that characterizes the drylands to the west. Ephemeral rivers running down to the Skeleton Coast cut through the north–south oriented mountain ranges leaving behind deep and narrow gorges, which alternate with wide interim basins (Fig. 1). In these valleys and basins fine-grained, mainly silty deposits indicate past periods of less rainfall and reduced sediment transport capacity of the rivers (Rust, 1989). In order to document Late Pleistocene and Holocene periods of climatic change the fine-grained fluvial deposits have been dated at several localities by radiocarbon isotopes and luminescence techniques in the Aba-Huab valley, the Huab valley, the Hoanib valley and the Hoarusib valley (Vogel and Rust, 1990; Eitel and Zöller, 1996; Eitel et al., 2001, 2002, 2005; Rust, 1999; Brunotte and Sander, 2000; Heine, 2004).

The fine-grained deposits show their greatest extension within the Hoanib River catchment. While the sediments in the Lower Hoanib valley around Amspoort have been well investigated (Rust, 1999; Eitel et al., 2005), the deposits in the upper and middle catchment area have not been studied systematically until now. In this paper we present new data for the fluvial sediments in the upper Hoanib River catchment, which are based on detailed field work, sedimentological analyses and the optical dating of 27 samples. The study provides information on changing palaeo-monsoon intensities at the eastern Namib Desert margin before and after the Last Glacial maximum (LGM).

2. Study area

The Hoanib River, which delineates the border between northern Damaraland in the south and Kaokoland in the north, has one of the largest catchment areas in northwestern Namibia (17,200 km^2). Like the Hoarusib River to the north and the Huab River further south, the Hoanib River originates from the semi-arid Etosha

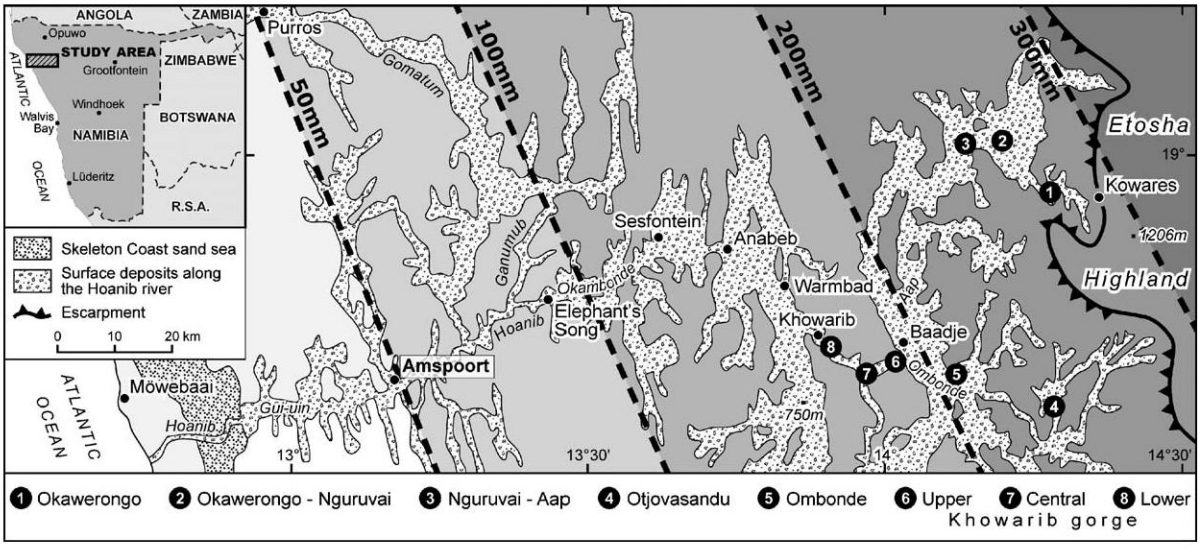

Fig. 1. The Hoanib River catchment in northwestern Namibia. The study concentrates on the upper catchment area down to the lower end of the Khowarib Gorge. The sampling locations are indicated with numbers 1–8.

Highland rim (200 – > 300 mm/a) in the east at ~1200 m a.s.l. (Fig. 1) and flows down to the Skeleton Coast where it breaks through the sand fields to the Atlantic Ocean every 5–10 years (Svendsen et al., 2003).

The Namibian highlands are hydrologically controlled by the summer rain that affects the eastern desert margin. Cyclonic excursions of the westerlies do not reach as far north as the study area at 19° S. Only from southern Namibia (Huns River, ~27° S) fine-grained deposits are known which may have formed under cyclonic (winter) rainfall conditions with weak runoff (Stengel and Leser, 2004). The pattern of convective summer rainfall is characterized by a high spatial and temporal variability resulting in seasonal runoff of variable magnitude. This is the reason why fine-grained sediments in the valleys can occur as thick river-end deposits (e.g. Rust, 1999; Eitel et al., 2001, 2005) or as slackwater deposits in backflood areas (e.g. Heine, 2004). The first type of sediments is due to drier conditions in the catchment area and low-energy runoff, whereas slackwater deposits are caused by high-energy runoff during more humid periods. The discussion has been summarized by Eitel et al. (2005).

It is assumed that the valleys and basins are very old landforms and date back possibly to the Palaeozoic (Martin, 1969; for critical comments see Spönemann and Brunotte, 2003). This is confirmed by remnants of Permian Dwyka tillites which occur in the Ombonde basin, the Okawerongo valley and the Otjovasandu valley as well as north of Anabeb in the western Warmbad basin (see Fig. 1). Since then, the forms of the basins and valleys have been essentially preserved, because they had been filled with sediments for the most part of the Mesozoic and the Cenozoic. In the Mesozoic they were most likely buried by central Gondwana sand- and siltstones, which were covered by Etendeka flood basalts (Stollhofen, 1999). These rocks were eroded during the Upper Cretaceous and the Lower Tertiary, and rivers cut epigenetic gorges (like the Khowarib Gorge) after the Atlantic Ocean had formed and humid climates prevailed. With the formation of the Benguela upwelling circulation in the eastern South Atlantic Ocean, southwestern Africa became drier and the basins in the upper Hoanib catchment were refilled by terrigenous deposits and calcretes of the Kalahari Formation (Upper Tertiary). Remnants of these calcretizised deposits still exist northwest of Warmbad and on top of the mountains north and east of the Aap and Ombonde Basin. Since the Pliocene or the Lower Quaternary exoreic drainage reworked the Tertiary deposits exposing large parts of the Palaeozoic land surface and drainage pattern again.

The present study focuses on the upper Hoanib River catchment area (Fig. 1) with the southern headstream of the Otjovasandu–Ombonde River and the Okawerongo–Aap River, which is the most important northern branch. Both tributary systems developed in Precambrian basement rocks. They join at Baadje to form the Hoanib River above the Khowarib Gorge, which cuts through the Damara dolomites (Precambrian–Cambrian). In the central parts of the Ombonde and the Aap basins, the thalweg is not much incised and the river tends to form 'vlaktes', i.e. accumulation areas where the runoff may terminate during drier seasons. As a consequence, it was only possible

Fig. 2. View to the ephemeral Nguruvai–Aap River near locality-3 (see Fig. 1). Note the greyish deposits of complex-I below the brownish sediment complex-II. (For interpretation of the references to colour in this figure legend, the reader is referred to the web version of this article.)

Fig. 3. View over the fine-grained deposits (complex-I) in the central Khowarib Gorge near locality-7 (see Fig. 1).

to gain samples at the fringe of the major basins, because in the 'vlaktes' themselves no natural exposures exist. This contrasts with the situation in the Okawerongo and Otjovasandu valleys, and the Khowarib Gorge where the Hoanib River has re-eroded different sediment-complexes to form deep erosion channels, which provide easily accessible natural profile walls (Figs. 2 and 3).

Although the dusty deposits have loess-like characteristics (Eitel et al., 2001) and may contain aeolian components, the well-stratified nature of the deposits indicates that they are of fluvial origin. They fill not only the main basins (Ombonde and Aap), but reach back upstream through the Khowarib Gorge into the highland tributary valley systems, which have flat to slightly inclined valley bottoms that end abruptly west of the Great Escarpment (see Fig. 1).

In the study area the valley and basin fills contrast strongly with the reddish, sandy and gravely riverbed material. The generally fine-grained deposits contain varying amounts of clay and silt, and minor contents of sand. This raises the question of age and formation of the silty fills, which are more or less eroded to river silt terraces (Eitel et al., 2001). The sediments are assumed to be important palaeoenvironmental markers as their deposition required less runoff than at present. While studies have already been published on the brownish surface deposits (Eitel et al., 2002) showing that these deposits formed during the Late Pleistocene and Holocene (Khowarib-II), until now no data existed for the older sedimentary complex below. This older sequence was first described by Eitel et al. (2001) as 'greyish Khowarib-I formation' after localities in the Khowarib Gorge, where it is well exposed.

3. Methods

Samples were taken in the upper Hoanib catchment area at eight representative sites (Fig. 1, Table 1), where the river has deeply eroded the deposits, naturally exposing several metres of the fine-grained sediment.

Table 1
Sample localities in the upper Hoanib catchment

Locality	Latitude/longitude	Height a.s.l.	Description
1	19°02′30″ S/14°16′40″ E	1098 m	Middle course of the Aap–Okawerongo River
2	18°58′25″ S/14°11′15″ E	1000 m	Confluence of the Aap–Okawerongo River and Nguruvai River (northern Aap Basin)
3	18°59′00″ S/14°08′51″ E	985 m	Aap–Nguruvai River (northeastern Aap Vlakte)
4	19°23′50″ S/14°17′ 01″ E	1020 m	Western branch of the Ombonde–Otjovasandu River (northwest of Kamdescha)
5	19°20′35″ S/14°07′17″ E	865 m	Ombonde Basin
6	19°18′30″ S/14°00′16″ E	800 m	Upper Khowarib Gorge
7	19°19′25″ S/13°59′00″ E	790 m	Central Khowarib Gorge
8	19°15′47″ S/13°53′30″ E	700 m	Lower Khowarib Gorge

3.1. Sedimentology

Sediment characteristics were determined at all eight locations. Sediment colour was specified using the Munsell Soil Color Chart and carbonate content was measured with a Scheibler apparatus. Particle size distribution was investigated after treatment with H_2O_2 and HCl, by sieving the grain-size fraction <2 mm and separating the silt and clay fractions through application of the Köhn/Köttgen method (Kretschmar, 1996). Heavy mineral identification of the fraction 0.063–0.2 mm in diameter, separated in an 80%-solution of sodium polytungstate (density 2.8 g/cm^3), was carried out using a petrographic microscope (Boenigk, 1983). Clay fractions were prepared by sedimentation in water. Oriented aggregates on glass targets, that were either air-dried, glycolated or heated to 550 °C, were analysed by X-ray diffraction (Velde, 1995).

3.2. Luminescence dating

OSL-ages were determined for 27 samples collected from the 8 study locations within the upper Hoanib catchment (Figs. 4–6). Apart from 2 aeolian samples (CL-1227, CL-1228) (Fig. 5) the material originates from fluvial deposits. While sample CL-1240 was taken from the coarse-grain sediments building up the subrecent 4 m-terrace (cf. Fig. 6), all the other fluvial samples originate from the older fine-grain deposits. OSL-samples were taken in light tight steel cylinders (Ø 55 mm). Care was taken to avoid obviously bioturbated or otherwise disturbed material. In the luminescence dark laboratory the outer, possibly light-influenced sedimentary rims (~1 cm) were removed and used for water-content and dose-rate determination. The interior samples were used for OSL-measurements.

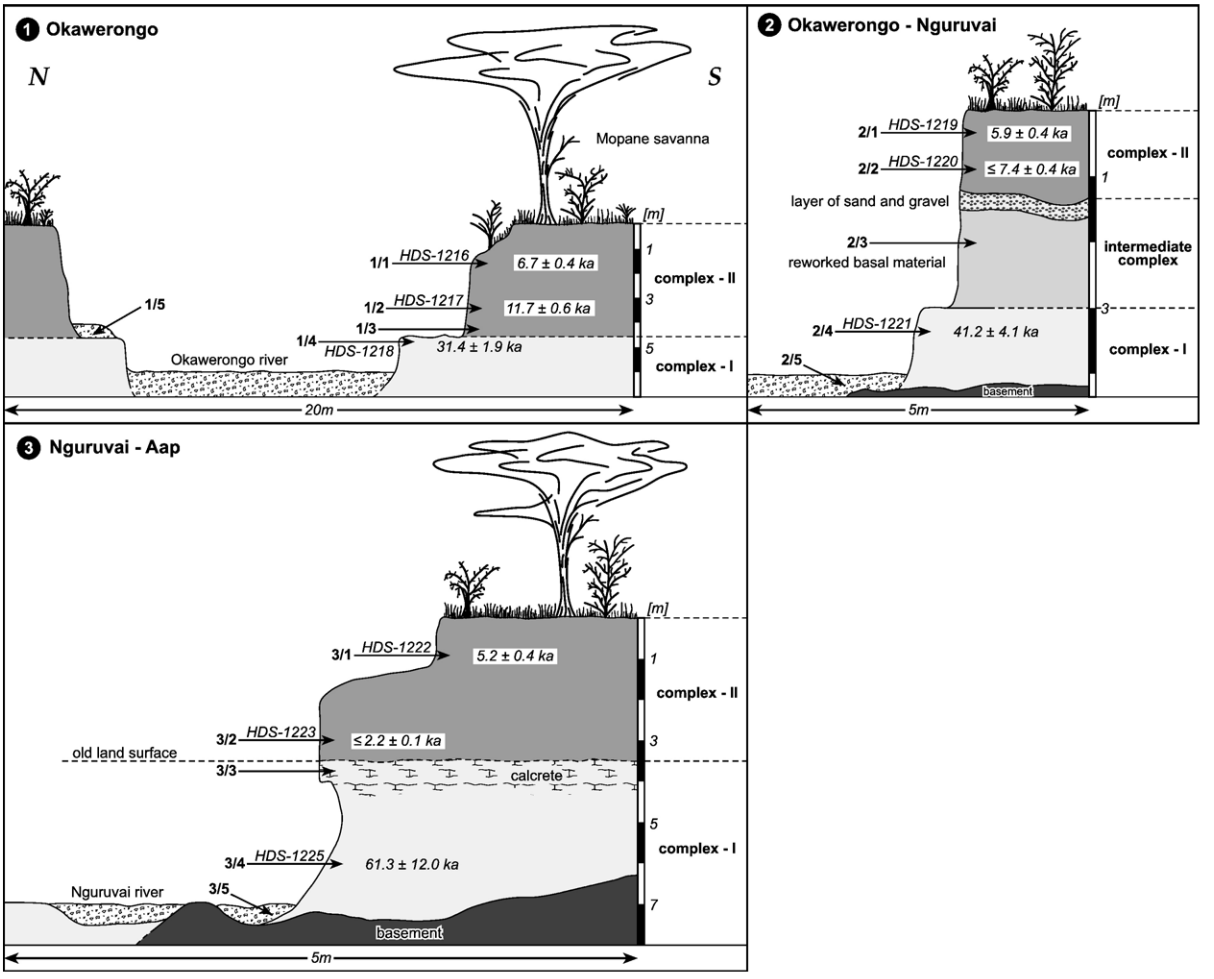

Fig. 4. Sketches and ages of the exposed layers at the localities 1–3 along the Okawerongo–Nguruvai–Aap River (northern Hoanib catchment, see Fig. 1).

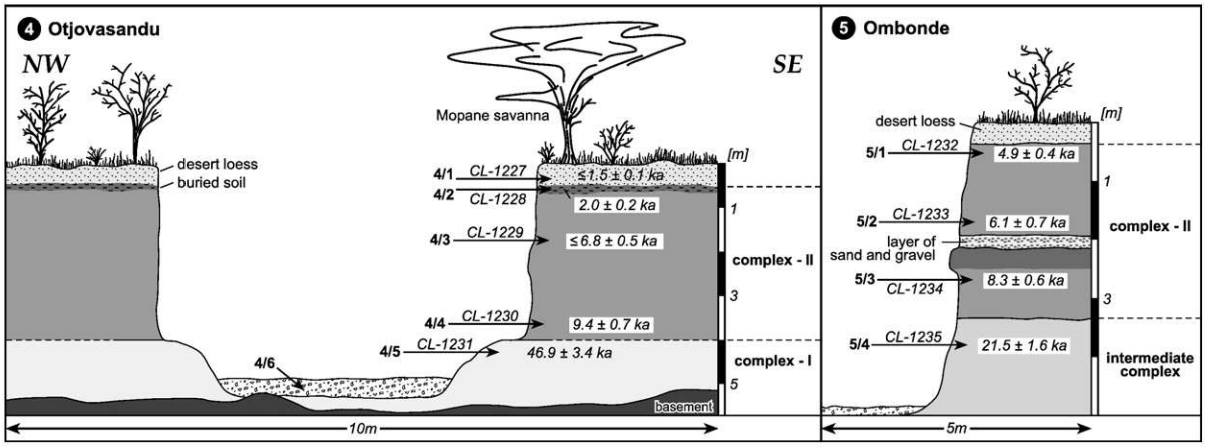

Fig. 5. Sketches of the exposed layers at the localities 4 and 5 along the Otjovasandu–Ombonde River (southern Hoanib catchment, see Fig. 1).

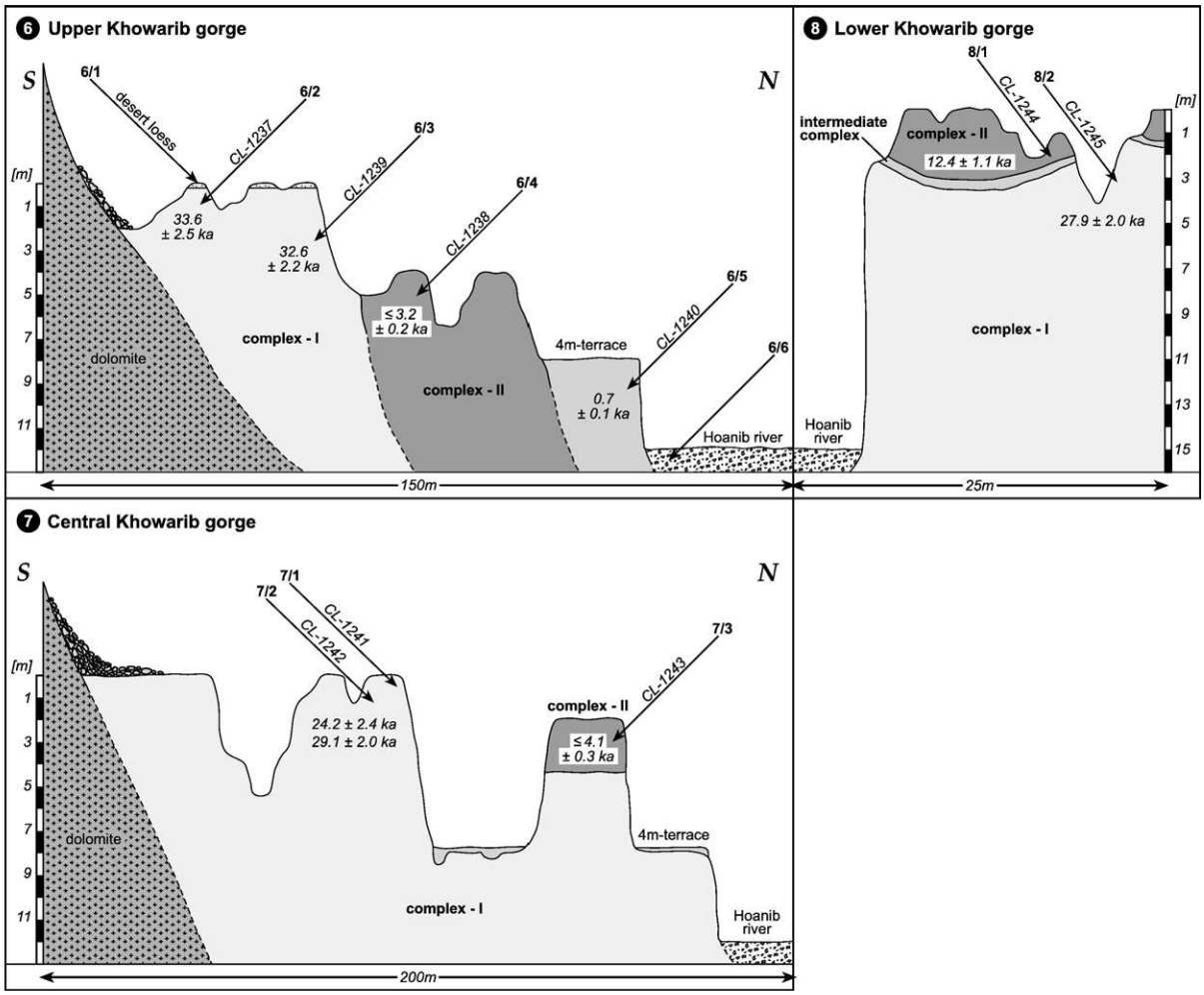

Fig. 6. Sketches of the exposed layers at the localities 6–8 in the Khowarib Gorge (upper Hoanib River, see Fig. 1).

OSL-sample preparation and OSL-dating were carried out in the luminescence laboratories of the Forschungsstelle Archäometrie of the Heidelberg Academy for the Humanities and Sciences (HDS-samples) and the Department of Geography of the University of Cologne (CL-samples). Handling occurred under extremely subdued red light (HDS-samples: Siemens LS5421-Q diodes covered by Hoya R62 glass filter (Schilles, 1998); CL-samples: Philips TL-D 36W/15).

As far as possible (20 samples) coarse-grain quartz-separates (~100–200 μm) were extracted for small-aliquot single-aliquot analyses (Table 4), which allow for the detection of insufficient bleaching of the mineral grains prior to deposition (e.g. Olley et al., 1998). If no coarse-grain quartz could be gained, either coarse-grain potassium feldspars (5 CL-samples) (Table 5) or polymineral fine-grains (HDS-1222, CL-1233) (Table 6) were analysed by luminescence techniques. Additional to coarse-grain quartz-analysis, for sample CL-1235 a coarse-grain potassium-feldspar separate was dated while for 8 further samples age-determinations were carried out for polymineral fine-grains (Tables 4–7).

Coarse-grain separates were extracted by wet sieving (grain size fractions 125–212 μm for HDS-samples) or dry sieving (100–200 μm for CL-samples), respectively. Polymineral fine-grains (4–11 μm) were taken from the sieved fraction <63 μm by means of density-separation from sediment-water suspensions either by using a water-cooled centrifuge followed by an additional separation of the material in acetone-filled test tubes (HDS-samples) or by using Atterberg cylinders (CL-samples). Carbonate and organic contents were removed by repeated reaction with HCl (10%, CL-samples) or CH_3COOH (20%, HDS-samples) and H_2O_2 (30%). Coarse-grain quartz and potassium feldspar extractions were carried out using lithium- (HDS-samples) or Na-polytungstate (CL-samples). In order to etch off the outer rim (~20 μm) of the mineral grains, which is possibly influenced by external α-irradiation, quartz-separates were etched in HF (40%, 40 or 45 min). The etched material was treated with HCl to remove any fluorides. The quartz coarse-grain fraction was finally separated by sieving off the particles <90 μm.

Fine-grain aliquots (~2 mg fine-grains per aliquot) were produced by pipetting a water-mineral-suspension onto aluminium discs (Ø 10 mm, 0.5 mm thick) with the fine-grains adhering to the plates after drying. Coarse-grain quartz and potassium-feldspar separates were created by fixing the mineral grains with silicon spray to aluminium cups (Ø 10 mm, HDS-samples) or steel plates (Ø 10 mm, CL-samples). As far as possible small aliquots containing ~200–500 grains, as suggested by Fuchs and Wagner (2003; HDS-samples), or ~150 grains (CL-samples) were used for D_E-determination. However, as the young sample CL-1240 produced only a weak luminescence signal, normal aliquots with about 1500–2000 grains had to be measured, which do not allow testing for insufficient bleaching (Tables 4 and 7).

IR-stimulated measurements of polymineral fine-grains (HDS-samples) were carried out on a Risø TL/OSL-reader DA12 (Bøtter-Jensen et al., 1991), which is equipped with a photomultiplier EMI9235Q for signal detection and a ring of TEMT484-diodes (880 Δ 80 nm) for IR-stimulation (~40 mW/cm^2). For the other OSL-measurements three TL/OSL-readers DA15 (Bøtter-Jensen, 1997) and one TL/OSL-reader DA12, upgraded to DA15, were used. The machines are equipped with calibrated $^{90}Sr/^{90}Y$-sources for β-irradiation (~5.2 Gy/min Heidelberg laboratory; ~7.0 and 12.9 and 1.0 Gy/min Cologne). The stimulation sources are clusters of 875 nm IR LEDs for IR-stimulation (~135 mW/cm^2) or rings of blue NISHIA NSPB-500 LEDs plus Schott GG-420 edge filter (470 Δ 20 nm) for blue light-stimulated luminescence (BLSL). Detection occurred with photomultipliers EMI9235QA coupled to filters for BLSL and IRSL measurements.

3.3. UV-detected BLSL SAR protocol for coarse-grain quartz-separates

For coarse-grain quartz-analyses the BLSL single-aliquot *regeneration* (SAR) protocol of Murray and Wintle (2000) was applied. Optical stimulation was carried out for 20 s (HDS-samples) or 50 s (CL-samples) at 125 °C (90% diode power) while the UV-component was detected using U-340 Hoya glass filters (7.5 mm). After reading out the natural signal, 3 to 5 regeneration doses bracketing the expected palaeodose were applied, before the smallest regeneration dose was repeated (test of reproducibility) and a zero dose point was measured. The luminescence signals of the regeneration dose points were normalised by the luminescence signals of intermittent test doses, which were ~0.4 Gy for HDS-samples and ~10% of the natural dose for CL-samples. A preheat of 10 s at 260 °C (HDS-samples) or 240–270 °C (CL-samples) was administered prior to luminescence readout of the natural or regenerated signals, while the cut-heat preceding stimulation of the test dose signal was held for 10 s at 160 °C. After finishing the SAR protocol, the aliquots were given the highest regeneration dose a second time and a usual preheat procedure was carried out, before an IR-stimulated signal was read out at room

temperature for 20 s in order to check the separates for possible feldspar contamination.

Of each sample 16 (HDS-samples) or 15–22 natural aliquots (CL-samples) were measured for D_E-determination. Measurements with a low reproducibility (recycling ratio <0.9 or >1.1) of the luminescence signal of the lowest dose point were eliminated from the D_E-data sets. OSL-ages were calculated based on the weighted mean of all D_E's and from the lowest D_E the apparent minimum age was calculated (Table 4).

For all of the HDS- and some of the CL-samples, dose recovery tests were carried out. For the HDS-samples, a set of 16 aliquots was bleached for 3 h under a Hönle solar simulator, where the sample holders were placed on a water-cooled copper plate and covered with a UVILEX glass filter. The natural luminescence signal of the CL-samples (CL-1240:16 aliquots, CL-1244: 12 aliquots) was bleached within the Risø reader by exposure to the blue diodes. The artificially bleached samples received a β-laboratory dose similar in size to the mean palaeodose gained from the set of natural aliquots. Finally the samples were measured with the same BLSL SAR protocol as the set of natural aliquots beforehand.

Dependency of D_E with preheat temperature was tested on two CL-samples. The aliquots of each sample were split into 4 groups (of 4 and 3 aliquots, respectively) and analysed using preheat temperatures of 220, 240, 260 and 280 °C, respectively. However, no dependency of the gained D_E-values on preheat temperature could be recognized. This result is in agreement with earlier preheat tests on coarse-grain quartz from the Hoanib River catchment, in which no dependency of D_E on preheat temperature was detected for aliquots carrying their natural BLSL signal (Eitel et al., 2005).

3.4. Blue-detected IRSL SAR protocol for coarse-grain potassium-feldspar separates

For D_E determination of the coarse-grain potassium feldspars, a SAR protocol (Murray and Wintle, 2000) was applied, similar to the protocol for coarse-grain quartz dating described above. This protocol was modified in terms of stimulation, signal detection and preheat temperatures following Wallinga et al. (2000) and Preusser (2003). IR-stimulation was carried out for 300 s at 125 °C (90% diode power). The luminescence

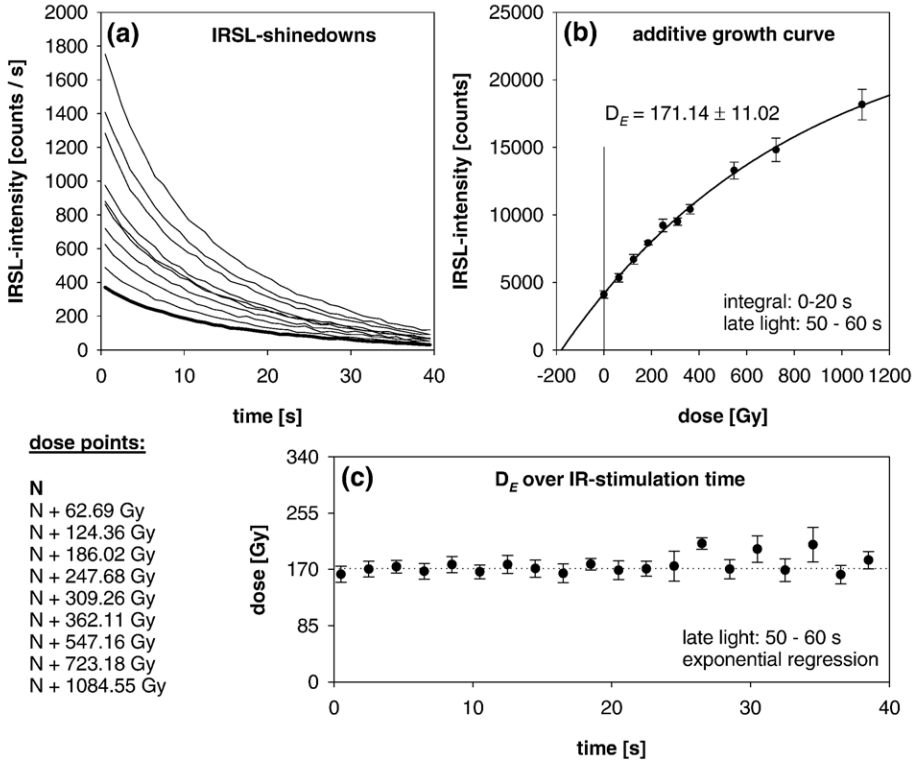

Fig. 7. D_E-determination for IR-stimulated polymineral fine-grains of sample HDS-1218 using a multiple-aliquot additive protocol. (a) IRSL-shinedown 0–40 s: each curve represents the mean of 10 natural or 5 additionally irradiated aliquots, respectively. (b) Additive growth curve using the integral 0–20 s after subtracting the late-light 50–60 s. (c) D_E-values versus IR-stimulation-time exhibiting a neat plateau. The broken line indicates the D_E-value of 171.1 ± 11.02 Gy.

signal was detected using a blue transmitting filter set (Schott BG 39, Schott GG 400, Corning 7–59). Preheat temperature following natural and artificial irradiation was set to 280 °C, while the cut heat following the test dose was set to 200 °C. 11–18 aliquots of each sample were measured for D_E-determination. No tests of anomalous signal fading were carried out.

3.5. Blue-detected IRSL MAAD protocol for polymineral fine-grains

For all of the HDS-samples polymineral fine-grain analyses were carried out with an infrared-stimulated multiple-aliquot additive protocol (e.g. Lang et al., 2003). The blue feldspar emission (410 nm) was detected using a glass filter combination of BG39/BG3/GG400/BG3 (Schott, 3 mm each; Krbetschek et al., 1996), whereas for the dim samples HDS-1219, HDS-1222 and HDS-1223 no normalisation procedures were used. For the other samples 0.4 s IR short-shines of the natural luminescence signals were applicated for inter-aliquot normalisation. For β-equivalent dose and a-value-determination external sources were used for β- ($^{90}Sr/^{90}Y$ sources, ~0.6 Gy/min and 9.4 Gy/min, respectively) and α-irradiation (^{241}Am source, ~4.2 Gy/min). The additive beta growth-curve above the natural signal (10 aliquots) was built up by (8 or) 9 additive dose points (5 aliquots each) spread at 0.3/0.7/1/1.3/1.7/2/3/4/(6) times of the expected palaeodose, while the luminescence α-efficiency was determined by 3 additive dose points (3 aliquots each) producing luminescence signals equivalent to the 1/2/3-fold additive β-dose equivalent (Fig. 7).

Table 2
Compilation of sedimentological data of the sediments at the localities 1–8

No.		Particle size [%]			Colour	$CaCO_3$ [%]	Clay minerals		
		Clay	Silt	Sand			Illite	Chlorite	Smectite
❶	1/1	21	43	36	10 YR 3/4	2	+++	–	
	1/2	21	43	36	10 YR 4/3	6	+++	–	
	1/3	20	38	42	10 YR 4/3	13	+++	±	
	1/4	19	40	41	2.5 R 5/2	10	+++	–	
	1/5	2	6	92	2.5 Y 4/4	<1	+++	–	
❷	2/1	44	40	16	10 YR 4/3	6	+++	±	
	2/2	55	35	10	10 YR 4/4	13	+++	++	
	2/3	45	26	29	10 YR 5/4	28	+++	++	
	2/4	50	34	16	2.5 YR 5/4	10	+++	+	
	2/5	2	3	95	5 YR 5/4	6	+++	±	
❸	3/1	49	38	13	10 YR 4/3	15	+++	±	
	3/2	42	25	33	10 YR 4/3	15	+++	±	
	3/3	68	24	8	(calcrete)	83	+++	++	
	3/4	42	33	25	2.5 Y 5/3	30	+++	++	
	3/5	3	2	95	5 YR 5/4	9	+++	±	
❹	4/1	17	56	27	10 YR 4/3	4	+++	–	
	4/2	11	59	30	10 YR 3/4	1	+++	–	
	4/3	18	32	50	10 YR 4/3	<1	+++	–	
	4/4	21	27	52	10 YR 4/4	<1	+++	–	
	4/5	9	44	47	2.5 Y 5/4	5	+++	±	
	4/6	1	3	96	7.5 YR 4/4	<1	+++	++	
❺	5/1	13	57	30	10 YR 4/4	1	+++	++	
	5/2	14	71	15	10 YR 4/2	1	+++	++	
	5/3	10	51	39	10 YR 4/3	<1	+++	++	
	5/4	17	52	31	10 YR 4/4	1	+++	++	
❻	6/1	48	26	26	2.5 Y 6/3	32	+++	+	±
	6/2	36	28	36	2.5 Y 6/3	32	+++	+	±
	6/3	72	28	0	5 Y 6/2	37	+++	+	±
	6/4	29	67	5	10 Y 4/4	6	+++	+	±
	6/5	13	34	53	7.5 YR 3/4	4	+++	–	–
	6/6	0	1	99	7.5 YR 4/4	1	+++	–	–
❼	7/1	51	39	10	2.5 YR 6/3	9	+++	±	
	7/2	75	23	2	2.5 YR 5/3	63	+++	+	
	7/3	34	59	7	10 YR 4/3	5	+++	++	
❽	8/1	42	31	27	10 YR 4/4	8	+++	±	
	8/2	60	29	11	2.5 YR 6.2	59	+++	±	

Table 3
Dose-rate data

Lab.-no.	Locality/ sample-no.	Depth b.g.l. [m]	Uranium[a] [μg/g]	Thorium[a] [μg/g]	Potassium[a] [weight %]	Water content			Effective dose rate
						Wet weight/dry weight measured [Δ]	Wet weight/dry weight modelled [Δ]		Coarse-grain *fine-grain*[b] [Gy/ka]
HDS-1216	1/1	0.5	4.53 ± 0.10	18.65 ± 0.22	2.86 ± 0.07	1.03	1.05 ± 0.05	Q	5.15 ± 0.29 *6.74 ± 0.33*
HDS-1217	1/2	1.6	4.61 ± 0.08	18.32 ± 0.22	2.74 ± 0.06	1.08	1.08 ± 0.05	Q	4.87 ± 0.27 *6.46 ± 0.25*
HDS-1218	1/4	1.2	3.38 ± 0.07	15.97 ± 0.19	2.29 ± 0.05	1.08	1.08 ± 0.05	Q	4.06 ± 0.22 *5.16 ± 0.19*
HDS-1219	2/1	0.3	3.52 ± 0.15	18.60 ± 0.63	2.55 ± 0.14	1.07	1.07 ± 0.05	Q	4.55 ± 0.27 *5.94 ± 0.25*
HDS-1220	2/2	0.8	4.19 ± 0.11	14.15 ± 0.22	2.13 ± 0.06	1.03	1.05 ± 0.05	Q	4.08 ± 0.23 *5.69 ± 0.24*
HDS-1221	2/4	3.3	5.64 ± 0.14	17.51 ± 0.30	2.72 ± 0.09	1.07	1.07 ± 0.05	Q	5.08 ± 0.29 *7.62 ± 0.48*
HDS-1222	3/1	1.0	3.90 ± 0.07	12.37 ± 0.17	2.30 ± 0.05	1.03	1.05 ± 0.05	–	– *5.18 ± 0.20*
HDS-1223	3/2	2.5	3.65 ± 0.13	10.13 ± 0.39	2.14 ± 0.11	1.03	1.05 ± 0.05	Q	3.68 ± 0.22 *5.12 ± 0.22*
HDS-1225	3/4	6.3	5.01 ± 0.12[c]	7.85 ± 0.14	1.60 ± 0.05	1.04	1.05 ± 0.05	Q Q	2.71 ± 0.19[c] 3.29 ± 0.19[c] *3.39 ± 0.17*[c] *4.31 ± 0.18*[c]
CL-1227	4/1	0.3	2.96 ± 0.33	17.80 ± 0.89	3.05 ± 0.15	1.01	1.02 ± 0.02	Q	4.94 ± 0.27 –
CL-1228	4/2	0.5	2.32 ± 0.26	15.60 ± 0.78	3.48 ± 0.17	1.01	1.02 ± 0.02	Q	5.04 ± 0.28 –
CL-1229	4/3	1.7	2.43 ± 0.27	15.70 ± 0.79	3.34 ± 0.17	1.02	1.02 ± 0.02	Q	4.91 ± 0.28 –
CL-1230	4/4	3.6	2.22 ± 0.24	15.90 ± 0.80	3.37 ± 0.17	1.02	1.02 ± 0.02	Q	4.86 ± 0.27 –
CL-1231	4/5	4.2	2.60 ± 0.29	15.30 ± 0.77	3.12 ± 0.16	1.02	1.02 ± 0.02	F	5.47 ± 0.28 –
CL-1232	5/1	0.5	2.70 ± 0.30	14.80 ± 0.74	2.58 ± 0.13	1.02	1.02 ± 0.02	Q	4.22 ± 0.23 –
CL-1233	5/2	1.6	2.43 ± 0.27	13.80 ± 0.69	2.23 ± 0.11	1.02	1.05 ± 0.05	–	– *5.15 ± 0.53*
CL-1234	5/3	2.4	2.47 ± 0.27	16.80±0.84	2.40 ± 0.12	1.01	1.02 ± 0.02	Q	4.09 ± 0.22 –
CL-1235	5/4	3.6	2.48 ± 0.27	15.70±0.79	2.61 ± 0.13	1.02	1.02 ± 0.02	Q F	4.19 ± 0.23 4.99 ± 0.25

Table 3 (*continued*)

Lab.-no.	Locality/ sample-no.	Depth b.g.l. [m]	Uranium[a] [μg/g]	Thorium[a] [μg/g]	Potassium[a] [weight %]	Water content			Effective dose rate
						Wet weight/dry weight measured [Δ]	Wet weight/dry weight modelled [Δ]		Coarse-grain *fine-grain*[b] [Gy/ka]
CL-1237	6/2	0.3	4.52 ± 0.27	6.88 ± 0.34	1.83 ± 0.09	1.19	1.20 ± 0.05	F	3.59 ± 0.20 –
CL-1238	6/4	0.6	2.12 ± 0.23	12.40 ± 0.62	2.37 ± 0.12	1.06	1.06 ± 0.03	Q	3.60 ± 0.19 –
CL-1239	6/3	2.0	7.06 ±0.35	9.84 ± 0.49	2.46 ± 0.12	1.22	1.20 ± 0.05	F	4.78 ± 0.22 –
CL-1240	6/5	0.8	1.88 ± 0.28	10.80 ± 0.54	1.99 ± 0.10	1.01	1.05 ± 0.05	Q	3.21 ± 0.18 –
CL-1241	7/1	0.3	2.72 ± 0.30	4.08 ± 0.20	0.78 ± 0.04	1.02	1.02 ± 0.02	F	2.49 ± 0.21 –
CL-1242	7/2	0.8	7.86 ± 0.39	7.75 ± 0.39	1.79 ± 0.09	1.20	1.20 ± 0.05	F	4.32 ± 0.21 –
CL-1243	7/3	0.5	2.25 ± 0.25	9.43 ± 0.47	1.92 ± 0.10	1.05	1.02 ± 0.02	Q	3.02 ± 0.18 –
CL-1244	8/1	1.0	1.46 ± 0.37	6.28 ± 0.31	1.63 ± 0.08	1.02	1.02 ± 0.02	Q	2.47 ± 0.17 –
CL-1245	8/2	2.0	6.77 ± 0.34	4.47 ± 0.22	1.18 ± 0.06	1.08	1.08 ± 0.04	Q	2.94 ± 0.15 –

The effective dose rate includes a contribution from cosmic radiation after Prescott and Hutton (1998).

[a] Determined by low-level gamma-spectrometry for HDS-samples and NAA for CL-samples.

[b] Q = quartz, F = feldspar.

[c] Sample showing radioactive disequilibrium in ^{238} U-chain, as detected by low-level gamma-spectrometry, possible minimum and maximum effective dose rates determined.

For tests of anomalous luminescence fading, a set of 5 aliquots with the natural luminescence signal and 5 additionally β-irradiated aliquots was prepared. Between laboratory irradiation and luminescence measurements the aliquots were stored at room temperature for 4 weeks. Within the Risø-reader a preheat of 300 s (older samples HDS-1218, HDS-1221 and HDS-1225 only) or 120 s at 220 °C was administered prior to IR-stimulation over 60 s. The early integral of the first 20 to 40 s of the shine-downs was used for D_E-determination, while the late-light 50–60 s was used for background subtraction (Aitken and Xie, 1992). Systematic investigations of D_E-values gained from successively earlier D_E-integrals (down to 0–1 s) and late-light integrals (down to 5–6 s) were carried out in order to examine possible partial bleaching (D_E-value plateau-test). The IRSL-signal of the aliquots used for the fading tests was read out after another ~2 months of dark storage at room temperature, i.e. after preheating and the actual measurements for palaeodose determination.

3.6. UV-detected post-IRSL BLSL SAR protocol for polymineral fine-grains

For sample CL-1233 a post-IRSL blue-stimulated SAR protocol was applied (Banerjee et al., 2001). Measurements (7 aliquots) were carried out on a Risø TL/OSL-reader DA15 (Bøtter-Jensen, 1997; see descriptions above). A preheat of 10 s at 270 °C was carried out prior to 100 s at 125 °C of IR-bleaching (90% diode-power), before the BLSL signal was read out for 100 s at 125 °C, while the quartz-dominated UV-luminescence signal was detected (U-340, 7.5 mm).

4. Results

4.1. Sedimentology

Particle size and sediment colour analyses show that different sedimentary units occur in the study area (Table 2). The actual river-bed is characterized

by sands which are coated by Fe-oxides. Sediment colours range from reddish brown (5 YR 4/4) to olive brown (2.5 YR 4/4). Such sands do not occur in the older deposits, which are divided into two complexes, (a) a basal complex-I with light olive brown (2.5 YR 5/3) to grey (5 YR 6/2) colours and (b) a generally dark (yellowish) brown complex-II. A second feature important to note is, that the basal sediments show often hydromorphic features, most likely due to water saturation when the complex-II was deposited above.

At every sampling location particle sizes show differences in composition between the two sedimentary complexes, but there is no clear trend. The fluvial sediments are fine-grained and mostly well laminated. Particles >2 mm in diameter are restricted to thin layers. According to the fluvial nature of the exposed deposits, both complexes are locally more clayey, silty or sandy indicating similar depositional environments. Carbonate contents vary strongly between <1% and 83% $CaCO_3$ for the calcrete sample. Minor amounts of carbonate occur in the deposits that fill the uppermost Hoanib tributary systems in the Okawerongo and Otjovasandu valleys (localities-1, -2, -4, and -5), while the deposits in the northern Aap Basin (locality-3) and in the Khowarib Gorge are very calcareous and reach >60% (localities-6, -7, and -8; see Fig. 1).

The heavy mineral compositions consist predominantly of epidote group minerals (>50%) with minor amounts of hornblende (green and brown) and pyroxene group minerals. Sphene and the stable minerals zircon and turmaline form very small fractions (~1%). The heavy minerals of complex-I are more weathered and show a greater abundance of oxidic coatings than the grains which were separated from samples of complex-II. The heavy minerals of the actual river-

Table 4
Dose data (artificially bleached samples), palaeodose data (natural samples) and OSL-ages of BLSL coarse-grain quartz-separates

Lab.-no.	Artificially dosed aliquots			Aliquots with natural luminescence signal					
	Applied D_E [Gy]	Recovered D_E with $1-\sigma$ SD and v		D_{Emean} with SD, v and skew[a]			Weighted D_{Emean}	Age from	
		[Gy]	[%]	[Gy]	[%]		[Gy]	Weighted D_{Emean} [ka]	D_{Emin} [ka]
HDS-1216	34.5	32.9 ± 0.8	2.5	34.6 ± 3.6	10.3	−0.2	34.2 ± 0.1	6.7 ± 0.4	5.5 ± 0.3
HDS-1217	58.7	56.0 ± 2.2	3.9	59.0 ± 1.7	11.4	0.5	57.2 ± 0.1	11.7 ± 0.6	9.9 ± 0.5
HDS-1218	166.4	166.8 ± 19.6	11.7	159.0 ± 10.3	24.1	0.7	127.3 ± 3.3	31.4 ± 1.9	28.0 ± 1.5
HDS-1219	28.0	27.0 ± 0.5	2.0	28.1 ± 1.4	19.9	0.8	26.8 ± 0.1	5.9 ± 0.4	4.8 ± 0.3
HDS-1220	31.0	29.8 ± 0.8	2.7	31.0 ± 1.3[b]	16.4	−0.1	28.9 ±0.1	7.4 ± 0.4	5.7 ± 0.3
HDS-1221	237.3	259.4 ± 34.3	13.2	209.0[a]	–	–	–	41.2 ± 4.1[a]	41.2 ± 4.1[a]
HDS-1223	10.8	11.0 ± 0.2	1.5	12.1 ± 1.8	59.3[c]	2.1	8.3 ± 0.01	2.2 ± 0.1	1.4 ± 0.1
HDS-1225	237.3	267.6 ± 22.9	8.5	237.2 ± 24.0	22.6	−0.1	179.7 ± 13.9	54.8 ± 2.9[d]	50.8 ± 2.9[d]
								66.4 ± 7.0	61.7 ± 4.4
CL-1227	–	–	–	7.4 ± 1.6	21.6	−0.3	7.2 ± 0.4	1.5 ± 0.1	0.8 ± 0.1
CL-1228	–	–	–	10.5 ± 1.4	13.7	1.3	10.2 ± 0.5	2.0 ± 0.2	1.7 ± 0.1
CL-1229	–	–	–	39.8 ± 10.6	26.6	0.3	33.2 ± 1.7	6.8 ± 0.5	4.1 ± 0.2
CL-1230	–	–	–	54.4 ± 12.4	22.8	1.1	45.7 ± 2.3	9.4 ± 0.7	8.0 ± 0.6
CL-1232	–	–	–	21.7 ± 3.0	13.7	0.3	20.6 ± 1.0	4.9 ± 0.4	4.2 ± 0.3
CL-1234	–	–	–	34.9 ± 5.1	14.9	0.9	34.0 ± 1.7	8.3 ± 0.6	6.7 ± 0.5
CL-1235	–	–	–	108.2 ± 29.3	27.1	0.3	90.0 ± 4.5	21.5 ± 1.6	16.5 ± 1.2
CL–1238	–	–	–	22.0 ± 18.7	84.9	2.5	11.4 ± 0.6	3.2 ± 0.2	1.8 ± 0.1
CL-1240[e]	1.6	1.6 ± 0.2	11.0	2.2 ± 0.5	23.7	0.7	2.1 ± 0.1	0.7 ± 0.1	0.5 ± 0.03
CL-1243	–	–	–	14.5 ± 3.9	26.9	0.3	12.4 ± 0.6	4.1 ± 0.3	2.7 ± 0.2
CL-1244	53.7	52.4 ± 5.9	11.3	30.5 ± 3.0	9.8	−0.4	30.6 ± 1.5	12.4 ± 1.1	10.0 ± 0.9
CL-1245	–	–	–	84.7 ± 11.0	13.0	0.6	82.0 ± 4.1	27.9 ± 2.0	23.7 ± 1.7

Note that for most of the samples, ages gained from the weighted mean of the D_E-values and the aliquot giving the corresponding lowest palaeodose are equal on the 2 σ error-level.

[a] Only one aliquot analysable not giving an infinite value (i.e. not beyond the scope of the SAR protocol).

[b] One extreme value of 194.3 ± 1.2 Gy excluded.

[c] Giving a v-value of 40.5% and a skewness of 0.7, if one extreme value above the highest dose point is excluded.

[d] Possible minimum and maximum age calculated according to radioactive disequilibrium.

[e] No small-aliquot analysis.

Table 5
IRSL SAR-ages of blue detected coarse-grain feldspar separates

Lab.-no.	Equivalent dose				Age from weighted D_{Emean} [ka]
	D_{Emean} [Gy]	v [%]	Skew	Weighted D_{Emean} [Gy]	
CL-1231	262.6 ± 32.0	12.2	0.4	256.4 ± 12.9	46.9 ± 3.4
CL-1235	102.9 ± 14.2	13.8	0.2	102.4 ± 5.2	20.5 ± 1.5
CL-1237	126.6 ± 20.2	16.0	0.6	120.8 ± 6.1	33.6 ± 2.5
CL-1239	157.9 ± 21.8	13.8	− 0.5	156.0 ± 8.0	32.6 ± 2.2
CL-1241	64.2 ± 20.4	31.9	− 0.3	60.2 ± 3.0	24.2 ± 2.4
CL-1242	123.1 ± 12.2	9.9	0.5	125.6 ± 6.3	29.1 ± 2.0

bed sands do not differ significantly from those of the valley fills.

The clay mineral assemblages are dominated by illite, which is accompanied by minor amounts of chlorite and smectites. Palygorskite could not be detected although the fibrous silicate is common in the nearby Tertiary deposits of the Etosha Highland (Eitel, 2000). Kaolinite is also absent.

4.2. Luminescence dating

Results of luminescence dating are presented in Tables 3–7 and Figs. 4–10. OSL-ages were calculated according to Gaussian error propagation, and errors are quoted on the $1-\sigma$ confidence interval. From all the HDS-samples investigated by low-level gamma-spectrometry, only sample HDS-1225 exhibits radioactive disequilibrium within the ^{238}U chain (Table 3), which is adequately addressed to by calculating possible maximum and minimum ages.

4.3. IRSL MAAD protocol for polymineral fine-grains (Table 6)

Sample HDS-1221 produces a failed D_E versus shinetime plateau, thus giving evidence of partial bleaching of the fine-grain component prior to deposition (Lang et al., 1999). Fading tests for samples HDS-1220 and HDS-1222 might indicate possible anomalous fading of the IR-stimulated luminescence signal (at least at the $1-\sigma$ confidence level).

4.4. BLSL SAR protocol for coarse-grain quartz

Samples measured with the BLSL SAR protocol exhibit steep shinedowns reaching a near zero background level after only 2–3 s of optical stimulation, produce well defined growth curves and show high reproducibilities of repeatedly measured dose points (Fig. 8). If samples exhibit an IR-stimulated signal after a repeated application of the highest dose point,

Table 6
OSL-age determination of polymineral fine-grain separates (all HDS-samples blue-detected IRSL-stimulation, multiple-aliquot additive protocol; sample CL-1233 UV-detected post-IRSL blue-stimulation, SAR-protocol)

Lab.-no.	Locality/sample-no.	D_E [Gy]	a-value	Fading [Δ]	Age [ka]
HDS-1216	1/1	32.1 ± 2.7	0.066 ± 0.011	0.91 ± 0.22	4.8 ± 0.5
HDS-1217	1/2	52.4 ± 3.3	0.069 ± 0.006	1.00 ± 0.08	8.1 ± 0.6
HDS-1218	1/4	171.1 ± 11.0	0.057 ± 0.004	0.99 ± 0.11	33.2 ± 2.5
HDS-1219	2/1	25.4 ± 1.5	0.070 ± 0.006	1.06 ± 0.22	4.3 ± 0.3
HDS-1220	2/2	40.1 ± 3.5	0.083 ± 0.007	0.81 ± 0.14	7.0 ± 0.7[a]
HDS-1221	2/4	393.5 ± 58.2[b]	0.112 ± 0.017	1.03 ± 0.08	51.6 ± 8.3[c]
HDS-1222	3/1	27.0 ± 1.8	0.060 ± 0.005	0.91 ± 0.17	5.2 ± 0.4
HDS-1223	3/2	28.2 ± 1.7	0.088 ± 0.005	1.05 ± 0.21	5.5 ± 0.4
HDS-1225	3/4	228.6 ± 17.9	0.056 ± 0.006	0.89 ± 0.08	53.1 ± 4.7[a,d] 67.5 ± 6.3
CL-1233	5/2	31.2 ± 1.7	0.070 ± 0.020[e]	–	6.1 ± 0.7

[a] Possible minimum age due to anomalous signal fading.
[b] Partial bleaching detected by failed plateau test (D_E versus stimulation/readout time), here: integral 0–1 s, late-light 50–60 s.
[c] Maximum age (partial bleaching).
[d] Possible minimum and maximum age calculated according to radioactive disequilibrium.
[e] a-value assumed.

Table 7
Compilation of OSL-ages

Lab.-no.	Field-no.	Coarse-grain separates				Polymineral fine-grains	
		BLSL, quartz SAR, UV-detection			IRSL, feldspar SAR, blue detection [ka]	IRSL, multiple aliquot additive protocol, blue detection [ka]	Post-IRSL BLSL, SAR, UV-detection [ka]
		Small aliquots [ka]		No small aliquots [ka]			
		$Age_{weighted\ mean}$ [ka]	$age_{minimum}$ [ka]				
HDS-1216	1/1	6.7 ± 0.4	5.5 ± 0.3	–	–	4.8 ± 0.5	–
HDS-1217	1/2	11.7 ± 0.6	9.9 ± 0.5	–	–	8.1 ± 0.6	–
HDS-1218	1/4	31.4 ± 1.9	28.0 ± 1.5	–	–	33.2 ± 2.5	–
HDS-1219	2/1	5.9 ± 0.4	4.8 ± 0.3	–	–	4.3 ± 0.3	–
HDS-1220	2/2	*7.4 ± 0.4*	*5.7 ± 0.3*	–	–	7.0 ± 0.7[a]	–
HDS-1221	2/4	(41.2 ± 4.1)[b]	(41.2 ± 4.1)[b]	–	–	51.6 ± 8.3[c]	–
HDS-1222	3/1	–	–	–	–	5.2 ± 0.4	–
HDS-1223	3/2	*2.2 ± 0.1*	*1.4 ± 0.1*	–	–	5.5 ± 0.4	–
HDS-1225	3/4	54.6 ± 5.2[d]	50.8 ± 2.9	–	–	53.1 ± 4.7[a,d]	–
		66.4 ± 7.0	61.7 ± 4.4	–	–	67.5 ± 6.3	–
CL-1227	4/1	*1.5 ± 0.1*	*0.8 ± 0.1*	–	–	–	–
CL-1228	4/2	2.0 ± 0.2	1.7 ± 0.1	–	–	–	–
CL-1229	4/3	*6.8 ± 0.5*	*4.1 ± 0.2*	–	–	–	–
CL-1230	4/4	9.4 ± 0.7	7.9 ± 0.6	–	–	–	–
CL-1231	4/5	–	–	–	46.9 ± 3.4	–	–
CL-1232	5/1	4.9 ± 0.4	4.2 ± 0.3	–	–	–	–
CL-1233	5/2	–	–	–	–	–	6.1 ± 0.7
CL-1234	5/3	8.3 ± 0.6	6.7 ± 0.5	–	–	–	–
CL-1235	5/4	21.5 ± 1.6	16.5 ± 1.2	–	20.5 ± 1.5	–	–
CL-1237	6/2	–	–	–	33.6 ± 2.5	–	–
CL-1238	6/4	*3.2 ± 0.2*	*1.8 ± 0.1*	–	–	–	–
CL-1239	6/3	–	–	–	32.6 ± 2.2	–	–
CL-1240	6/5	–	–	0.7 ± 0.1	–	–	–
CL-1241	7/1	–	–	–	24.2 ± 2.4	–	–
CL-1242	7/2	–	–	–	29.1 ± 2.0	–	–
CL-1243	7/3	*4.1 ± 0.3*	*2.7 ± 0.2*	–	–	–	–
CL-1244	8/1	12.4 ± 1.1	10.0 ± 0.9	–	–	–	–
CL-1245	8/2	27.9 ± 2.0	23.7 ± 1.7	–	–	–	–

For coarse-grain quartz-separates that were analysed by a small-aliquot SAR-protocol, the weighted mean ages ($age_{weighted\ mean}$) and the age gained from the aliquot delivering the lowest palaeodose ($age_{minimum}$) are given. Significantly differing ages are italicised.

[a] Possible minimum age due to anomalous signal fading.

[b] Only one aliquot analysable.

[c] Maximum age (partial bleaching).

[d] Possible minimum and maximum age calculated according to radioactive disequilibrium.

the strength is negligible (<2% of the blue stimulated natural signal).

In the dose recovery tests all laboratory doses given to artificially bleached samples are recovered within the $1-$ or $2-\sigma$ range of the standard deviation of the mean, indicating the good quality of the BLSL SAR protocol with respect to dose determination from quartz-separates (Table 4; Fig. 9). Dose recoveries based on small-aliquot measurements show high precision of the obtained results with coefficients of variation v (i.e. (standard deviation/mean) × 100) ranging for most of the HDS-samples between 1.5% and 3.9%. The relatively wide scatter of v-values (8.5% to 13.2%) of samples HDS-1218, HDS-1221 and HDS-1225 results from the high doses which are fitted into the saturating and thus less precisely defined part of the growth curves. Coefficients of variation of >10% are usually encountered also for artificially thoroughly bleached samples, if small aliquots with only ~100 grains are measured (Fuchs and Wagner, 2003) as is the case with sample CL-1244.

However, predominantly high scatter in D_E-values is observed with regard to the aliquots carrying the natural luminescence signal. Apart from CL-1244 all samples possess v-values >10%, which with respect to small-aliquot analyses of coarse-grain quartz-separates is generally considered as a threshold value pointing to insufficient bleaching prior to deposition (Clarke, 1996;

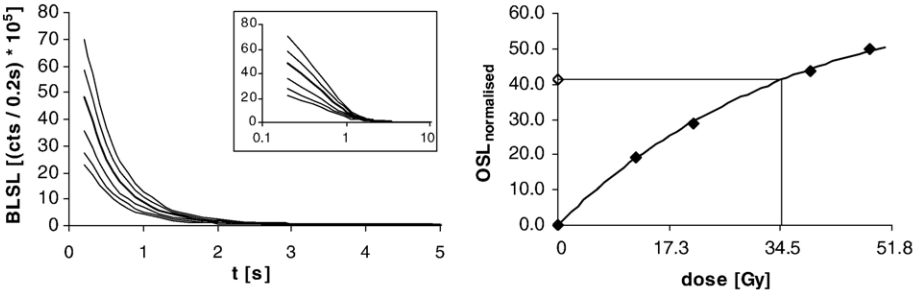

Fig. 8. D_E-determination for one aliquot of sample HDS-1220 using a BLSL single-aliquot regenerative (SAR) protocol. BLSL-shinedowns (left) and regenerative growth curve (right) (for details see text).

Fuchs and Wagner, 2003). Insufficient bleaching is also indicated by v-values from natural samples which are significantly larger than those gained from artificially bleached samples. Yet, there are reasons to assume that the OSL-ages meet the order of the true ages.

(1) OSL-ages are stratigraphically consistent at all of the sampled localities.
(2) For none of the HDS-samples, which have been analysed both by BLSL on coarse-grain quartz and IRSL on fine-grains does the coarse-grain quartz age overestimate the corresponding fine-grain age. Apart from sample HDS-1223, for which bleaching of the fine-grain component was obviously less sufficient than for the coarse-grain deposit, the minimum quartz ages fall within the $2-\sigma$ error range of the polymineral fine-grains. It seems rather unlikely, that the same ages would be produced for two different fractions of a significantly badly bleached and therefore age-overestimated sediment.
(3) Similar considerations also apply to sample CL-1235, which yields consistent ages for coarse-grain IRSL feldspar- and BLSL quartz-separates (20.5 ± 1.5 ka and 21.5 ± 1.6 ka, respectively).
(4) At locality-6, complex-I sediments were sampled from two different nearby positions. Coarse-grain IRSL feldspar analyses yielded identical ages (33.6 ± 2.5 ka for CL-1237 and 32.6 ± 2.2 ka for CL-1239).
(5) At locality-7 too, complex-I sediments were collected from two different nearby places, for which the two IRSL feldspar-ages are in agreement (25.3 ± 2.5 ka for CL-1241 and 29.1 ± 2.0 ka for CL-1242).
(6) Sample CL-1240 originates from the material making up the 4 m-terrace at locality-6. The BLSL age of 0.7 ± 0.1 ka produced from normal coarse-grain quartz aliquots is in agreement with ^{14}C-ages published by Heine (2004).
(7) Eitel et al. (2005) report OSL-ages of fine-grained fluvial deposits from sampling sites further downstream the Hoanib valley, which had been accumulated during the Little Ice Age period. Although these samples, too, give indication of insufficient bleaching, they are in agreement with independent calibrated radiocarbon ages.
(8) Additionally, OSL-ages from this study are in agreement with OSL-ages for other fluvial deposits in the ephemerally flooded Hoarusib and the Khumib valleys (Srivastava et al., 2004, 2005). From the standard-errors of the palaeodoses given in these studies for all the presented 18 samples v-values may be derived well above the threshold value of 10% pointing to heterogeneous bleaching prior to deposition. Yet, here too, the chronometrical results deliver stratigraphically consistent ages clustering in distinct periods (for further discussion of the palaeo-geoecological significance of these concordances see below).

Thus, in spite of the indication of differential bleaching, OSL-ages gained from the fluvial deposits of the upper Hoanib catchment area give reliable numerical estimates of the true sedimentation periods.

5. Discussion

The analytical results support the field observation of two distinct sediment complexes filling the valleys and basins of the upper Hoanib catchment area. They do not differ significantly in their mineral composition, as they reflect essentially the local metamorphic rocks. Some brown hornblende points to the volcanic Etendeka basalts as being a source in the southern catchment area.

The well laminated fine-grained structure of the deposits indicates low-energy runoff of the rivers during sedimentation. Complete covering of the basin and

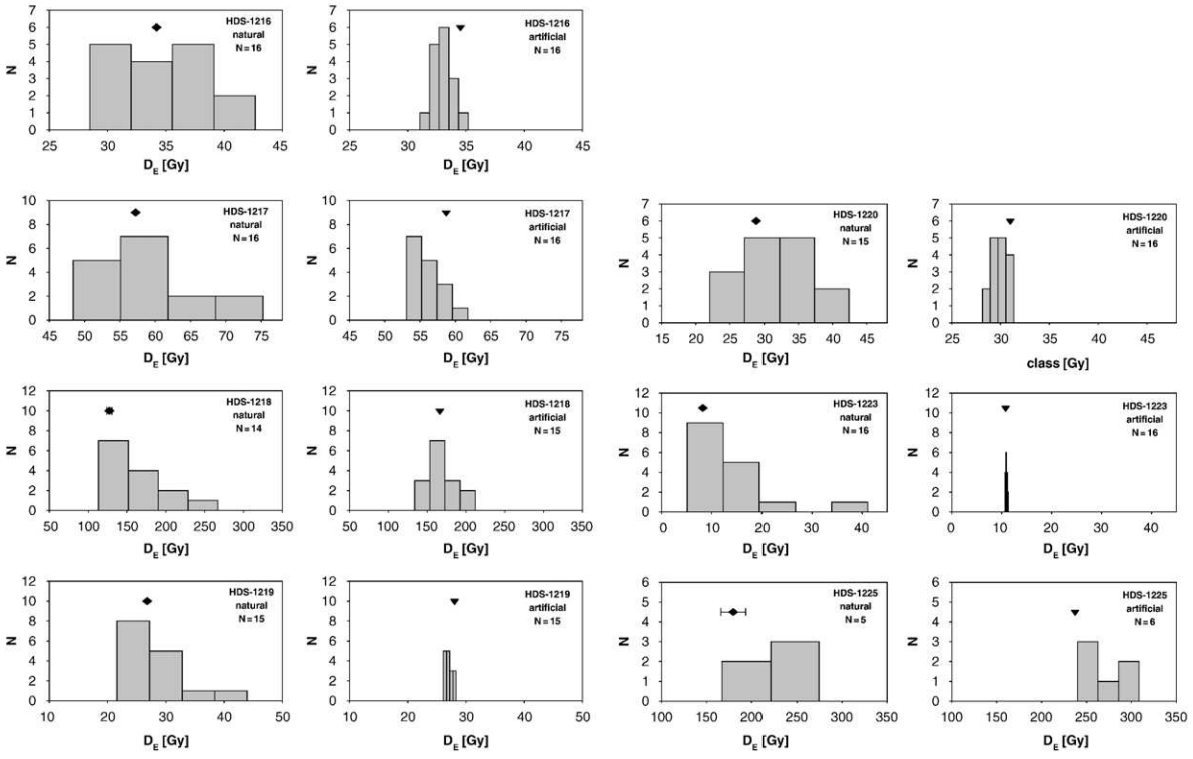

Fig. 9. Histograms of BLSL SAR analyses (small aliquots) of coarse-grain quartz-separates of all HDS-samples (with the exception of sample HDS-1221, which yielded only one analysable aliquot). For each sample, measurements of natural aliquots are shown on the left and of artificially bleached and dosed aliquots on the right. Bin width was set to the standard deviation of the unweighted D_E-mean of the corresponding SAR measurements. Also shown are the weighted D_E-means of the natural samples (black diamonds) and the applied, i.e. expected doses of the artificially treated aliquots (black triangles). The graphs demonstrate the relatively higher scatter of the natural samples, which suggests partial bleaching. As smaller D_E-values (from better bleached aliquots) are extracted from the initial, steeper part of the exponential growth curve, they usually possess a smaller error than higher D_E-values (from poorly bleached aliquots). Therefore, weighted means of D_E-values from natural samples usually rather lie in the initial part of the D_E-value distributions. This seems reasonable for partially bleached sediments. Note that for artificially bleached and dosed samples, the expected D_E-values are met by the weighted means of D_E-values (cf. Table 4), but they are usually underestimated by the lowest D_E-bin of the histograms (with the exception of sample HDS-1225). If there is no clear indication of partial bleaching, D_E-extraction from a leading edge of a D_E-value distribution could be problematic and lead to age underestimation. This is not the case with the present samples, as in most cases the ages gained from the lowest measured D_E-values and corresponding weighted means of D_E-values are consistent on the 2 σ error-level (cf. Tables 4 and 7).

valley bottoms excludes repeated high-energy slackwater deposition in backflood positions as it was suggested for similar deposits in northwestern Namibia (Heine, 2004; Srivastava et al., 2004). The changing character of the deposits, sometimes more clayey, silty or sandy, indicates weak runoff oscillations. According to the high spatial and temporal variability of the monsoonal summer rains, the rivers carried a lot of load in suspension that derived from local weathering products, but – in general – the runoff had not enough competence to transport coarse sands, pebbles or even boulders. Flowing west to the arid northern Namib Desert, runoff became increasingly weak, seeped away and – controlled by the water supply – the sediment load has been deposited at a range of end-points. The sediment complexes-I and -II are due to endoreic discharge confirming the idea that the rainfall was triggered by monsoonal influences from the east and not by westerlies that must have affected the whole coastal desert. Such river-end deposition has been considered responsible for similar deposits further downstream in the Hoanib River (Rust, 1999; Eitel et al., 2001, 2005). The deposition of only the fine-grained sediments in the upper catchment area excludes the notion that the river has crossed the Namib Desert for longer periods and discharged into the Atlantic Ocean as is suggested by Heine (2004). At present, the river incises seasonally, forming deep channels, and it reaches the Atlantic Ocean once every 5–10 years. Therefore the sediment complexes-I and -II give evidence of drier climatic conditions with less intense rainfall events in the past.

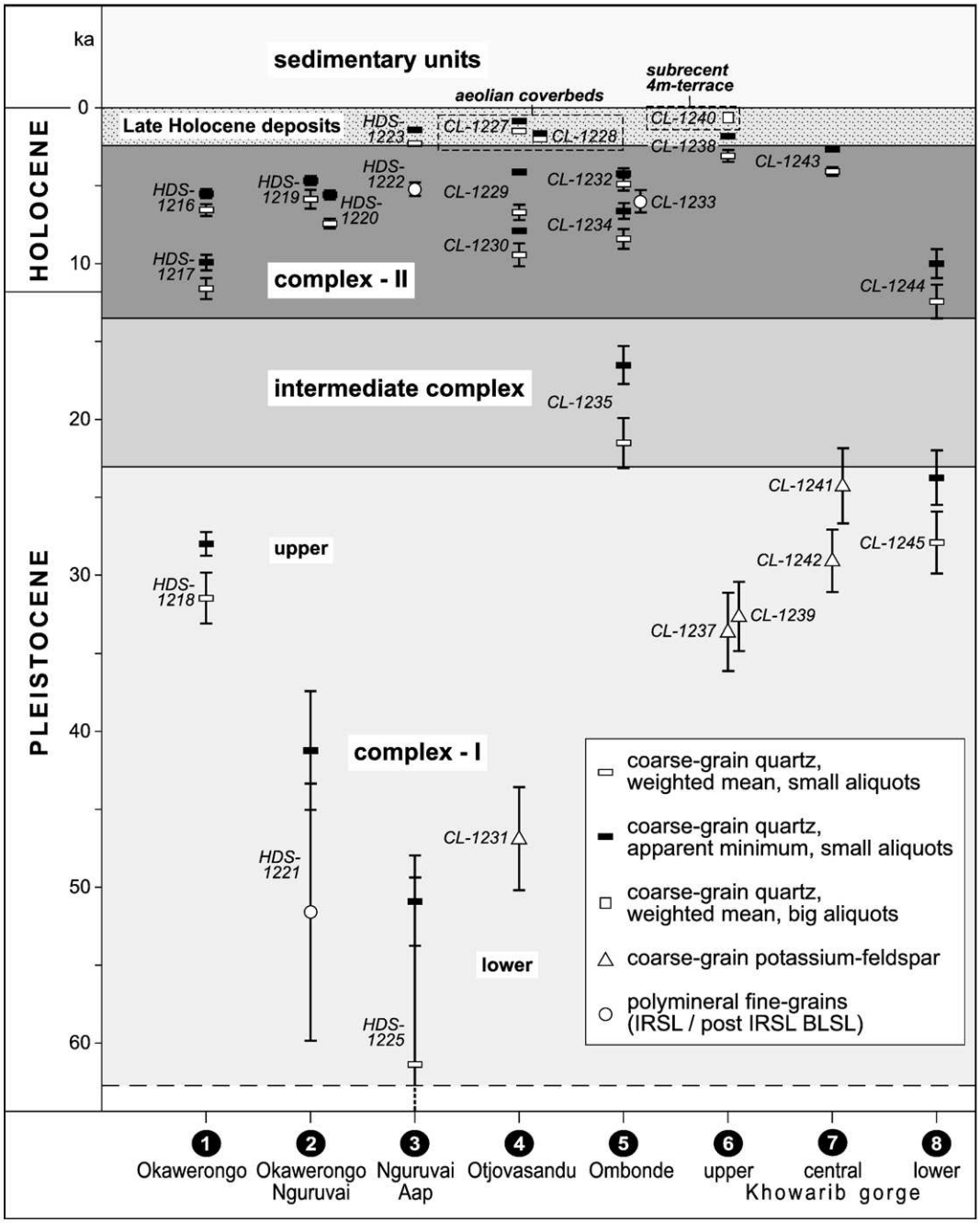

Fig. 10. Compilation of all luminescence ages at the localities 1–8.

5.1. Complex-I

Complex-I is the oldest sediment sequence within the upper Hoanib catchment area (for Khowarib Gorge identical with 'Khowarib-I' silts according to Eitel et al., 2001, and 'silt member 1' according to Heine, 2004). It is more consolidated and more hardened than complex-II. The light, sometimes greyish colours are caused by higher carbonate contents (5–63%) and by hydromorphic bleaching, while the hydromorphic oxides concentrate in patches and stripes. At present the sediments of this complex are dry. We suggest that iron dynamics started when the basins and valleys were seasonally flooded and complex-II was accumulated above, and it may still go on after heavy rains in the summer season.

Luminescence ages grossly correspond to Oxygen Isotope Stage 3 (OIS 3). The oldest sediments were sampled at the eastern margin of the northern Aap Basin (cf. locality-2 and -3; see Fig. 1). They accumulated not before 61.3 ± 12.0 ka (HDS-1225; age rather imprecise due to radioactive disequilibrium) and 41.2 ± 4.1 ka (HDS-1221) and in the Otjovasandu valley (locality-4, see Fig. 1) at 46.9 ± 3.4 ka (CL-1231). All three localities are proximal to the rocky basement outcrops visible in the actual river bed indicating, that we sampled the lowest (oldest) sedimentary unit.

It is most likely that the upper part of complex-I had been eroded before complex-II was deposited, because some exposures show reworked materials (e.g. intermediate complex at locality-2) separating the brownish layers of complex-II from the underlaying greyish complex-I. Downstream of Baadje (Fig. 1) the dark brown deposits of complex-II fill erosion channels, which are incised in complex-I (see locality-6, Fig. 6). At the localities-6 and -7 the uppermost and youngest parts of complex-I are exposed. Deposition occurred between ~24 and ~34 ka ago (CL-1237, CL-1239, CL-1241, CL-1242, CL-1245, cf. Table 7 and Fig. 6). This correlates with the ages of the greyish complex-I exposed in the Okawerongo valley (HDS-1218) and the lower Khowarib Gorge (HDS-1245).

Until now only one other locality was known in northwestern Namibia where fluvial deposits occur which accumulated during the same period as complex-I. The Clay Castle Silts in the middle Hoarusib catchment area, adjoining the Hoanib drainage system to the north, are suggested to have formed at ~44–40 ka and ~29–20 ka ago. They were interpreted as stillwater deposits in shaded backflood positions (Srivastava et al., 2005), or as river-end deposits due to low-energy runoff and caused by drier conditions at the desert margin (Rust and Vogel, 1988). However, Rust and Vogel (1988) also report rather high ages for the Clay Castle Silt formation (>40 ka BP, beyond the range of radiocarbon ages). It is important to note that the Clay Castle Silt formation consists of two sediment aggradation phases, which coincide with the accumulation of complex-I in the upper Hoanib catchment area.

In the Hoanib River catchment area complex-I formed during a period of weak runoff which deposited mainly fine-grained, dusty sediments already in the valleys and basins of the upper catchment area. This is in contrast to the hydrological conditions with more pronounced runoff at present. Therefore, it is most likely that before the Late Glacial Maximum monsoonal summer rains reached the Hoanib catchment only marginally and the region was somewhat drier than at present. During most of the humid seasons, the Hoanib River ended within its upper catchment area forming river-end deposits (complex-I). From this follows that the arid coastal desert strip was 40–60 km wider than at present.

Complex-I sediments are calcareous. At locality-3 (Fig. 4), a pedogenic calcrete covers the basal complex-I giving strong evidence that sedimentation was interrupted over a longer period. The calcrete formation indicates a rainfall deficit and an ancient land surface with soil formation and subsoil carbonate accumulation (Blümel, 1982; Eitel, 1994). The hardening to a hardpan calcrete (Netterberg, 1969) requires exhumation of the subsoil horizon and dry conditions and point to post-sedimentary aridification (Blümel, 1991; Fedoroff and Courty, 1999). It is most likely that this dry phase coincides with the LGM after the deposition of the top layer of complex-I at ~24 ka.

5.2. Intermediate complex

The basal parts of complex-II often contain reworked material derived from complex-I. This material has been distinguished as an 'intermediate layer' or 'intermediate complex'. At locality-2 dating failed, but at locality-5 deposition occurred ~22 ka ago (CL-1235, 21.5 ± 1.6 ka for BLSL quartz and 20.5 ± 1.5 ka for IRSL feldspar, respectively; cf. Table 7). This age is an outlier and belongs neither to the formation period of complex-I nor to complex-II (Fig. 10).

5.3. Complex-II

Most materials of complex-II are also river-end deposits. They are not restricted to backflood positions but are widespread along the river courses in the upper and middle Hoanib catchment area. In contrast to complex-I, which ends at Khowarib, the dark brown complex-II forms the top of the basin fills down to the Okambonde Vlakte upstream of Elephants Song (Fig. 1). Runoff must have varied more widely than during complex-I deposition. This includes repeated sediment removal, transport and re-deposition further downstream. Luminescence dating is affected by these processes as revealed by high coefficients of variation (v) indicating differential bleaching. Nevertheless, OSL-ages point to a Holocene formation of complex-II (~12–3 ka; cf. Fig. 10). This agrees with the only age published for complex-II sediments in the upper Khowarib Gorge (~9 ka; Eitel et al., 2001) and with dates from similar deposits in the Ombonde Basin (~3.4 and 6.4 ka, Eitel et al., 2002).

5.4. Late Holocene deposits

Younger sedimentation processes are indicated by aeolian coverbeds, mostly desert loess (e.g. at locality-4), and a fluvial 4 m-terrace (e.g. at locality-6, Fig. 6). The aeolian sediments are widespread in the upper Hoanib catchment area. At locality-4 in the Otjovasandu drainage system they occur twice, as an older layer pedogenetically overprinted (CL-1228, $\leq 2.0 \pm 0.2$ ka; cf. Table 7) and as unconsolidated loess (CL-1227, $\leq 1.5 \pm 0.1$ ka; cf. Table 7). It is possible that this indicates a Late Holocene period of increased loess deposition when the Hoanib River and its tributaries incised and removed large quantities of the fine-grained silty deposits of complex-I and -II. It is likely that the period with intensified loess formation at the eastern Namib Desert margin is not restricted to the Hoanib catchment, because similar loess deposits are known from the upper Huab valley further south (Garubib Farm, Eitel et al., 2002).

The 4 m-terrace in the upper Khowarib Gorge (locality-6) is built up by sediments deriving from fluvial flash floods which characterize the ephemeral rivers in the study area at present. The deposits consist of gravely, sandy and silty layers which are reworked materials from the older sedimentary complexes in the vicinity. The structure of the deposits indicates repeated high-energy runoff. The thin silty layers and lenses in this terrace resemble slackwater deposits as suggested by Heine (2004) for the widespread occurrences e.g. in the Orange valley (southern Namib Desert), but it must be noted that the vertical structure of the terrace in total is very different from the more homogenous and very thick silty river-end deposits in complexes-I and -II. Radiocarbon ages show that the terrace in the Khowarib Gorge formed during the past centuries (Heine, 2004). Our OSL-age from locality-6 confirms this (CL-1240, 0.7 ± 0.1 ka). In contrast to the Amspoort Silts (Lower Hoanib valley), which formed during the Little Ice Age (Rust, 1999; Eitel et al., 2005) the question remains open, whether the young Khowarib terrace is due to special Little Ice Age conditions too (Heine, 2004), because drift wood on top of it gives evidence of – at least – episodically flooding of the terrace at present. This includes partial reworking of sediments.

6. Conclusion

The compilation of all data including results from previous studies provides a more detailed chronology of past environmental changes in northwestern Namibia (Fig. 11) than has previously existed.

- The Hoanib complex-I indicates weak monsoonal summer rain and sediment aggradation which most likely occurred in two phases, between 60–40 ka and ~34–24 ka. For the first time this gives an idea of the monsoonal activity over the northwestern highlands of Namibia during Marine Isotope Stage 3 (MIS 3). The sediments provide evidence that the climate was semi-arid but drier than at present. Rainfall came from the east and affected not the coastal Namib Desert but its eastern margin. This led only to weak runoff and river-end deposits in the eastern part of the Hoanib drainage system. If the tropical wind circulation system followed the existing pattern, we can conclude that the monsoonal influence was less strong than at present in southwestern Africa.
- There is general consensus that during the Last Glacial Maximum very dry conditions prevailed in southwestern Africa (cf. the synopsis by Partridge et al., 1999; Eitel et al., 2002; Eitel, 2005; Shaw and Thomas, 2005). Desert environments expanded and fluvial activity in the drainage systems west of the Great Escarpment was interrupted. This is also indicated by the high carbonate content of the complex-I sediments and calcrete formation at its top. These findings correspond to similar soil–sediment complexes in the upper Aba-Huab river catchment area further south (Eitel and Zöller, 1996), which also point to geomorphic stability and pedogenesis during the LGM.
- As gullying of complex-I is observed at several locations (cf. Heine, 2004) fluvial erosion must have preceded the deposition of complex-II in the latest Pleistocene and Early to Mid-Holocene. Evidence of humid conditions was also derived from palynological and sedimentological records from marine core GeoB1023, which shows repeated oscillations between arid and humid conditions during the Late Pleistocene (Shi et al., 2000).
- The aggradation of complex-II started after ~12 ka and peaked between 9–5 ka. It is not restricted to the uppermost Hoanib River catchment area but reaches downstream at least until Elephants Song (Fig. 1). Repeated partial reworking of complex-I sediments, which are embedded at the base of complex-II ('intermediate complex'), indicate that the magnitude of runoff events must have oscillated over a wider range than during the formation of complex-I. The findings show that during the Early to Mid-Holocene a semi-arid climate prevailed that was drier than

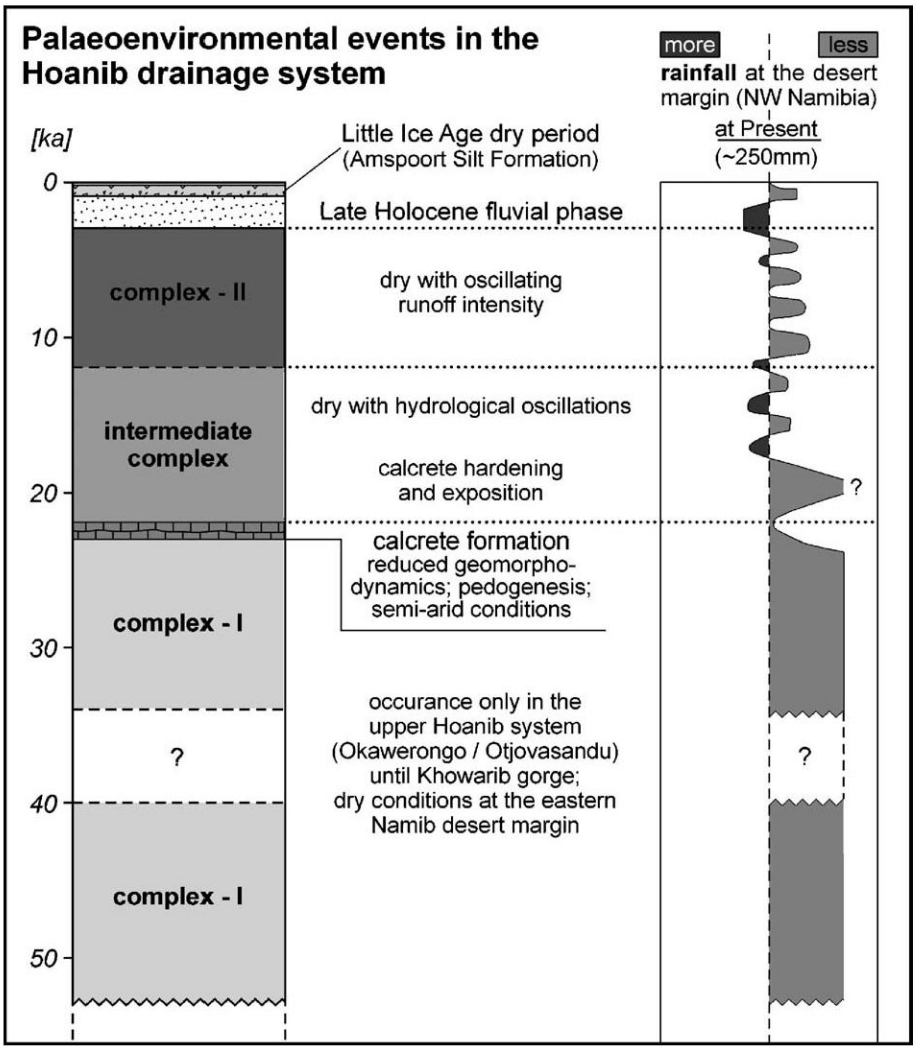

Fig. 11. Sediment stratigraphy and palaeoenvironmental interpretation.

present, but less stable and with more hydrological oscillations than before the LGM. In the Hoanib valley the sediments of complex-II can document this process of erosion and downstream redeposition.

- After ~3 ka the climate became significantly more humid at the eastern desert margin and the Hoanib River deeply eroded the two sediment complexes along its course to the Atlantic Ocean.
- The 4 m-terrace is the next youngest sedimentary unit, which probably accumulated during the Little Ice Age (cf. also Heine, 2004). The deposit is much coarser than the river-end complexes-I and -II and consists of more sandy and gravely materials. It is possible that the aggradation of the coarse 4 m-terrace sediments in the middle Hoanib River valley is correlated with the Amspoort Silts formation in the Lower Hoanib valley, which are river-end deposits that formed between the 14th and the 19th century AD (Rust, 1999; Eitel et al., 2005).
- At present the conditions east of the Namib Desert are too humid for (major) fluvial sediment accumulation. Erosional processes prevail, resulting in progressive terrace consumption.

Acknowledgements

As part of the geomorphological project 'Hygric fluctuations in northwestern Namiba' and connected with the IGCP 413 on dryland environmental changes, the study was generously supported by the German Science Foundation (Deutsche Forschungsgemeinschaft, DFG). We thank B. Chase and P. Kershaw for critical comments, S. Lindauer and A. Al-Karghuli for their assistance in the laboratory, Volker Schniepp for

designing several figures, and E. Roberts, who helped to improve the English.

References

Aitken, M.J., Xie, J., 1992. Optical dating using infrared diodes: young samples. Quaternary Science Reviews 11, 147–152.

Banerjee, D., Murray, A.S., Bøtter-Jensen, L., Lang, A., 2001. Equivalent dose estimation using a single aliquot of polymineral fine grains. Radiation Measurements 33, 73–94.

Boenigk, W., 1983. Schwermineralanalyse. Enke, Stuttgart.

Blümel, W.D., 1982. Calcrete in Namibia and SE-Spain. Relations to substratum, soil formation and geomorphic factors. Catena. Supplement 1, 67–82.

Blümel, W.D., 1991. Kalkkrusten-Ihre genetischen Beziehungen zu Bodenbildung und äolischer Sedimentation. Geomethodica 16, 169–197.

Bøtter-Jensen, L., 1997. Luminescence techniques: instrumentation and methods. Radiation Measurements 27, 749–768.

Bøtter-Jensen, L., Ditlefsen, C., Mejdahl, V., 1991. Combined OSL (infrared) and TL studies of feldspars. Nuclear Tracks and Radiation Measurements 18, 257–263.

Brunotte, E., Sander, E., 2000. Löss accumulation and soil formation in Kaokoland (Northern Namibia) as indicators of Quaternary climatic change. Global and Planetary Change 26, 67–75.

Clarke, M.L., 1996. IRSl dating of sands: bleaching characteristics at deposition inferred from the use of single aliquots. Radiation Measurements 26, 611–620.

Eitel, B., 1994. Kalkreiche Decksedimente und Kalkkrustengenerationen in Namibia: Zur Frage der Herkunft und Mobilisierung des Calciumcarbonats. Stuttgarter Geographische Studien 123, 1–193.

Eitel, B., 2000. Different amounts of pedogenic palygorskite in South West African Cenozoic calcretes: geomorphological, palaeoclimatical and methodological implications. Zeitschrift für Geomorphologie. Supplementband 121, 139–149.

Eitel, B., 2005. Environmental history of the Namib Desert. In: Smith, M., Hesse, P. (Eds.), 23° S — Archaeology and Environmental History of the Southern Deserts. National Museum of Australia Press, Canberra, pp. 29–44.

Eitel, B., Zöller, L., 1996. Soils and sediments in the basin of Dieprivier-Uitskot (Khorixas District/Namibia): age, geomorphic and sedimentological investigation, paleoclimatic interpretation. Palaeoecology of Africa and Surrounding Islands 24, 159–172.

Eitel, B., Blümel, W.D., Hüser, K., Mauz, B., 2001. Dust and loessic alluvial deposits in northwestern Namibia (Damaraland, Kaokoveld): sedimentology and palaeoclimatic evidence based on luminescence data. Quaternary International 76/77, 57–65.

Eitel, B., Blümel, W.D., Hüser, K., 2002. Environmental transitions between 22 ka and 8 ka in monsoonally influenced Namibia — a preliminary chronology. Zeitschrift für Geomorphologie. Supplementband 126, 31–57.

Eitel, B., Kadereit, A., Blümel, W.D., Hüser, K., Kromer, B., 2005. The Amspoort Silts, northern Namib desert (Namibia): formation, age and palaeoclimatic evidence of river-end deposits. Geomorphology 64, 299–314.

Fedoroff, N., Courty, M.A., 1999. Soil and soil forming processes under increasing aridity. In: Singhvi, A.K., Derbyshire, E. (Eds.), Palaeoenvironmental Reconstruction in Arid Lands. Elsevier, Amsterdam, pp. 73–108.

Fuchs, M., Wagner, G.A., 2003. Recognition of insufficient bleaching by small aliquots of quartz for reconstructing soil erosion in Greece. Quaternary Science Reviews 22, 1161–1167.

Grün, R., Wintle, A. (Eds.), Proceedings of the Tenth International Conference on Luminescence and Electron Spin Resonance Dating- LED 02. Quaternaty Science Reviews 22, 1–1382.

Heine, K., 2004. Little Ice Age climatic fluctuations in the Namib Desert, Namibia, and adjacent areas: evidence of exceptionally large floods from slack water deposits and desert soil sequences. Lecture Notes in Earth Sciences 102, 137–165.

Krbetschek, M.R., Rieser, U., Stolz, W., 1996. Optical dating: some luminescence properties of natural feldspars. Radiation Protection Dosimetry 66 (1–4), 407–412.

Kretschmar, R., 1996. Kulturtechnisch-bodenkundliches Praktikum. Ausgewählte Labor-und Feldmethoden vol. 1. Univ. Kiel, Kiel.

Lang, A., Kadereit, A., Behrends, R.-H., Wagner, G.A., 1999. Optical dating of anthropogenic sediments at the archaeological site of Herrenbrunnenbuckel, Bretten-Bauerbach (Germany). Archaeometry 41, 397–411.

Lang, A., Hatté, C., Rousseau, D.D., Antoine, P., Fontugne, M., Zöller, L., Hambach, U., 2003. High-resolution chronologies for loess: comparing AMS ^{14}C and optical dating results. Quaternary Science Reviews 22, 953–959.

Martin, H., 1969. Paläomorphologische Formelemente in den Landschaften Südwest-Afrikas. Geologische Rundschau 58, 121–128.

Murray, A.S., Wintle, A.G., 2000. Luminescence dating of quartz using an improved single-aliquot regenerative-dose protocol. Radiation Measurements 32, 57–73.

Netterberg, F., 1969. The interpretation of some basic calrete types. South African Archaeological Bulletin 24, 117–122.

Olley, J., Caitcheon, G., Murray, A., 1998. The distribution of apparent dose determined by optically stimulated luminescence in small aliquots of fluvial quartz: implications for dating young sediments. Quaternary Geochronology 17, 1033–1040.

Partridge, T.C., Scott, L., Hamilton, J.E., 1999. Synthetic reconstruction of Southern African environments during the Last Glacial Maximum (21–18 kyr) and the Holocene Altithermal (8–6 kyr). Quaternary International 57/58, 207–214.

Prescott, J.R., Hutton, J.T., 1998. Cosmic ray and gamma ray dosimetry for TL and ESR. Nuclear Tracks and Radiation Measurements 14 (1/2), 223–227.

Preusser, F., 2003. IRSL dating of K-rich feldspars using the SAR protocol: comparison with independent age control. Ancient TL 21 (1), 17–23.

Rust, U., 1989. (Palão)-Klima und Relief: Das Reliefgefüge der südwestafrikanischen Namibwüste (Kunenz bis 27° s Br.). Münchner Geographische Abhandlungen 7, 1–158.

Rust, U., 1999. River-end deposits along the Hoanib-River, northern Namib: archives of Late Holocene climatic variation on a subregional scale. South African Journal of Science 95, 205–208.

Rust, U., Vogel, J.C., 1988. Late Quaternary environmental changes in the Namib Desert as evidenced by fluvial Landforms. Palaeoecology of Africa 19, 127–137.

Schilles, Th., 1998. Entwicklung und Anwendung einer Technik zur 'Single Aliquot' Datierung mittels optisch stimulierter Lumineszenz. Diplomarbeit (Diplom-thesis), Fakultät für Physik und Astronomie, University of Heidelberg, Germany.

Shaw, P.A., Thomas, D.S.G., 2005. Late Quaternary environmental change in the Kalahari. In: Smith, M., Hesse, P. (Eds.), 23°S — Archaeology and Environmental History of the Southern Deserts. National Museum of Australia Press, Canberra, pp. 29–44.

Shi, N., Dupont, L.M., Beug, H.-J., Schneider, R., 2000. Correlation between vegetation in Southwestern Africa and oceanic upwelling in the past 21,000 years. Quaternary Research 54, 72–80.

Spönemann, J., Brunotte, E., 2003. Palaeozoic valley systems in Namibia? New aspects: morphogenetic contradictions and morphotectonic relations. Zbl. Geol. Paläont. Teil I, 2002/1–2, 97-115.

Srivastava, P., Brook, G.A., Marais, E., 2004. A record of fluvial aggradation in the northern Namib Desert margin during the Late Pleistocene–Holocene. Zeitschrift für Geomorphologie. Supplementband 133, 1–18.

Srivastava, P., Brook, G.A., Marais, E., 2005. Depositional environment and luminescence chronology of the Hoarusib River Clay Castle sediments, northern Namib Desert, Namibia. Catena 59, 187–204.

Stengel, I., Leser, H., 2004. Late Quaternary valley-fill terraces and palaeoenvironments of the Huns River, Southern Namibia. Die Erde 135, 129–149.

Stollhofen, H., 1999. Karoo Synrift-Sedimentation und ihre tektonische Kontrolle am entstehenden Kontinentalrand Namibias. Zeitschrift der Deutschen Geologischen Gesellschaft 149, 519–632.

Svendsen, J., Stollhofen, H., Krapf, C.B.E., Stanistreet, I.G., 2003. Mass and hyperconcentrated flow deposits record, dune damming and catastrophic breakthrough of ephemeral rivers, Skeleton Coast Erg, Namibia. Sedimentary Geology 160 (1–3), 7–31.

Van der Merve, J.H., 1983. National Atlas of South West Africa (Namibia). Stellenbosch (92 sheets).

Velde, B., 1995. Composition and origin of clays. In: Velde, B. (Ed.), Origin and Mineralogy of Clays. Clays and Environment. Springer, Heidelberg/Berlin, pp. 8–42.

Vogel, J.C., Rust, U., 1990. Ein in der kleinen Eiszeit (Little Ice Age) begrabener Wald in der nördlichen Namib. Berliner Geographische Studien 30, 15–34.

Wallinga, J., Murray, A.S., Wintle, A.G., 2000. The single-aliquot regenerative-dose (SAR) protocol applied to coarse-grain feldspar. Radiation Measurements 32, 529–533.